energies

MDPI

*Article*

# A Study of the Impact of Methanol, Ethanol and the Miller Cycle on a Gasoline Engine

**Luke Oxenham and Yaodong Wang ***

Department of Engineering, Durham University, Durham DH1 3LE, UK; luke.oxenham@durham.ac.uk
* Correspondence: yaodong.wang@durham.ac.uk

**Abstract:** This paper focuses on the investigation and optimisation of the Miller cycle, methanol, ethanol and turbocharging when applied to a high-performance gasoline engine. These technologies have been applied both individually and concurrently to test for potential compounding effects. Improvements have been targeted with regards to both emission output and performance. Also assessed is the capability of the engine to operate when exclusively powered by biofuels. This has been carried out numerically using the 1D gas dynamics tool 'WAVE', a 1D Navier–Stokes equation solver. These technologies have been implemented within the McLaren M838T 3.8L twin-turbo engine. The Miller cycle early intake valve close (EIVC) improved peak efficiency by 0.17% and increased power output at low and medium loads by 11%. Reductions of 6% for both $NO_x$ and CO were also found at rated speed. The biofuels achieved $NO_x$ and CO reductions of 60% and 96% respectively, alongside an efficiency increase of 2.5%. Exclusive biofuel use was found to be feasible with a minimum 35% power penalty. Applied cooperatively, the Miller cycle and biofuels were not detrimental to each other, compounding effects of a further 0.05% efficiency and 2% $NO_x$ improvements were achieved.

**Keywords:** miller cycle; methanol; ethanol; petrol engine; turbocharger



**Citation:** Oxenham, L.; Wang, Y. A Study of the Impact of Methanol, Ethanol and the Miller Cycle on a Gasoline Engine. *Energies* **2021**, *14*, 4847. https://doi.org/10.3390/en14164847

Academic Editor: Ulugbek Azimov

Received: 13 July 2021
Accepted: 5 August 2021
Published: 9 August 2021



## 1. Introduction

Relative improvements in gasoline engine efficiency over recent years have been driven by the tightening of global legislation. This was instigated by a larger scientific awareness of our environment's condition and eventual development path, at the current rate of carbon production [1]. Legislative changes began back in the 1960s, however the tightening has grown increasingly since then to meet the imminent and constrictive global emissions targets [2]. There are major concerns surrounding the production of several forms of emission:

- Carbon dioxide ($CO_2$), currently the most abundant greenhouse gas (GHG), largely due to fossil fuel combustion and as such is a significant global warming contributor [1].
- Nitrogen oxides ($NO_x$), a large indirect contributor to smog production and acid deposition. The US EPA reported a 51% output reduction from 1990 to 2014 [3].
- Carbon monoxide (CO), which causes an indirect increase in methane within the atmosphere, a prevalent GHG [4].
- Hydrocarbons (HC), such as methane, although emitted significantly less than $CO_2$ it is a potent GHG that warms the atmosphere 84 times more strongly than $CO_2$ over a period of 20 years [5].

The Paris Agreement set out in 2015 the limitation of global warming temperatures to under 2 °C, mainly by the restriction of carbon dioxide output [6]. The UK's contribution was to target net zero GHG output by 2050. In terms of road vehicles, the emission of carbon from a gasoline engine is unavoidable as gasoline is a carbon based fuel. Cars contribute 17% of all carbon based emissions in the UK, while all road vehicles output 27.4%

of the UK's total [7]. Therefore, limitations in this area have the potential to significantly reduce the impact of the UK's carbon output.

The Miller cycle, theorised by Ralph Miller in 1957, is a simple adjustment to the 4-stroke cycle, in which the intake valve timing is changed [8]. This is such that the valve will be closed either early or late with respect to the baseline profile [9]. This has the effect of decoupling the expansion ratio from the compression ratio [10]. As such, the compression stroke is shortened relative to the expansion with no change made to the expansion process [9]. The ability to improve efficiency, reduce emissions [11] and improve power output at select loads with no inherent cost is very appealing to manufacturers.

Biofuel use within gasoline engines has been a topic of interest for manufacturers since the 1970s [12]; this report has targeted the use of methanol and ethanol as blends with gasoline. Although widely used in small fractions, large fraction usage has so far been dismissed due to power loss and the corrosiveness of the liquids [13]. It is theorised that the shorter hydrocarbon chains and net reduction of gasoline will result in a reduction of the formation of $CO_2$ and usage of the fossil fuel [14]. Alcohols by nature are also a renewable resource, extracted from renewable microbial biomass, providing a more sustainable solution to vehicular transportation [15]. Methanol is synthesised from the syngas produced from renewable biomass, however the technology to form the syngas is still in development [15]. Ethanol, on the other hand, can be mass produced from the fermentation of carbohydrates, most commonly corn starch [15]. There is potential with these fuels to greatly reduce a variety of emissions and improve thermal efficiency.

This report ultimately aims to contribute to the reduction of GHG emissions and fossil fuel usage, aiding manufacturers in meeting current and future legislative targets. Investigations and optimisations of a variety of biofuel blends and Miller cycle implementations have taken place. Although past literature has widely covered investigation of these technologies [9–12,14], consideration of high performance engines with the Miller cycle and in particular high mass fraction blends is yet to be researched. The engine of consideration in this report therefore provides a unique research opportunity for environmental concerns of an engine with speeds and power exceeding 7500 RPM and 400 kW respectively. These investigations have tested the Miller cycle and biofuel's viability for practical application and potential for environmental impact reduction. This report also details the progressive proposal of operating the two technologies concurrently. Attempts to utilise the increased pressure induced with the Miller cycle alongside an increased octane fuel blend is yet to be considered in past literature. Incremental simulations have taken place in attempts to yield a positive impact. Guan [16] discussed this potential in 2020 with a diesel engine, however gasoline engine investigation has very little backing in past literature. As such, this project aims to be a breakthrough in the understanding of the combination potential.

These investigations have been carried out within Ricardo's 1D gas dynamics tool 'WAVE', a 1D Navier–Stokes equation solver [17]. The two technologies of concern—the Miller cycle and renewable biofuels—were applied to the McLaren M838T engine model within the software. To understand the impact of varying implementations, they were applied incrementally, from small valve timing changes/mass fraction blends up to extreme application. This was done to understand the variation in benefits and any optimum solutions. Through simulation the impact of these technologies on a variety of mechanical and emission outputs has been recorded across all operational engine loads. These simulations have been compared and contrasted to find implementations of high potential.

## 2. Theory and Method

### *2.1. Miller Cycle Theory*

Two variations of intake valve manipulation were developed by Ralph Miller in 1957, with the intention of maximising the work extracted from the combustion cycle: the early intake valve close (EIVC) and late intake valve close (LIVC) [18]. The Miller cycle is compatible with both 2- and 4-stroke cycles, in this case the basis will be 4-stroke. For

this to be implemented, changes need to be made to the intake valve lift profile during crankshaft rotation. This is achieved by the use of variable valve timing (VVT). Intake valve lift profiles are altered from the baseline by varying degrees of early or late closure. Figure 1a shows an example of each. These profiles have the effect of decoupling the expansion ratio from the compression ratio, in which the compression ratio is reduced relative to expansion. This is achieved exclusively by alterations in the compression stroke, in which a period of blow-back shortens the compression period. From Figure 1b, this period of blow-back can be seen between points 2 and 2′. For the EIVC this occurs due to the closure of the intake valve part way through the expansion process from TDC to BDC (1 to 2). As no air–fuel mixture enters between 2′ and 2, no work is done through compression in that period and compression is shortened. For the LIVC, this blow-back occurs as the intake valve remains open as the piston rises from BDC in compression (2 to 3′), causing a loss of charge through the valve and no work done between 2 and 2′.

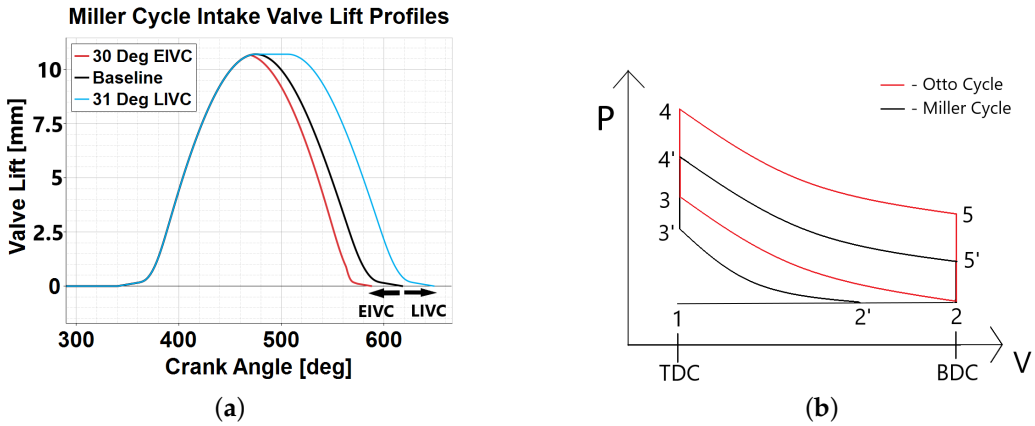


**Figure 1.** Miller cycle variable valve timing (created within Ricardo's WAVE and Microsoft Word). (**a**) Intake Valve Profiles; (**b**) Pressure-Volume Characteristics.

The Miller cycle may be adopted for a variety of reasons, all of which stem from the ability to lower the effective compression ratio as compared to the geometric compression ratio, without affecting the expansion ratio. Pan [10] found that increased intake advance angle (EIVC) caused increased knock suppression tendency. The Miller cycle can also reduce both peak in-cylinder temperature and charge temperature following compression [10]. This is due to a reduction in the high-temperature exhaust gases re-entering the cylinder on the intake stroke and as a result the temperature of charge prior to combustion is reduced. As stated by Pan this is beneficial to combustion, improving efficiency, and lowering cylinder temperature, limiting $NO_x$ formation [11]. Demirci [8] reported a maximum decrease in $NO_x$ emissions of 7.79%. The reduced temperatures however can promote incomplete combustion, thus increasing output of hydrocarbons (HC) and carbon monoxide (CO). Demirci [8] also reported an increase of HC and CO emissions of 6.48% and 11.66%, respectively. The Miller cycle has the potential to improve both fuel economy and engine efficiency. This is due to the Miller cycle enabling increased work to be extracted from the expanding gases as they expand to near atmospheric pressure [19]. The reduction of friction losses contributes to increased efficiency. This mostly concerns LIVC in which cylinder pressures are reduced [10]. Pan showed a direct correlation between the EIVC and increased pumping mean effective pressure (PMEP), causing significant reductions in pumping losses, thus increasing engine efficiency. A major drawback however of the Miller cycle is the power output deficiency, primarily at high load. Demirci [8] reported a loss of power following Miller cycle implementation for all engine speeds: 5.24% of brake torque and 1.17% of brake engine power. This was found to be due to the loss of charge air during the Miller cycle, primarily an issue for LIVC implementation. A further cause is the increase in opposing pressure formed as the piston rises to TDC. In addition, the reduction in combustion duration limits positive pressure post TDC for EIVC [20]. Although it is

overall beneficial to implement turbocharging alongside the Miller cycle to compensate for this power loss, Pan [10] found that the introduced back-pressure from turbocharging somewhat limits the pumping loss decrease from the Miller cycle. The turbocharging achieves air compensation within the cylinder that was otherwise lost through blow-back or early closure.

### *2.2. Renewable Biofuel Theory*

As the transportation sector looks to switch to a more sustainable future the two renewable biofuels investigated in this report have the potential to play a vital role. Petroleum reserves in the Earth's crust are limited. Both methanol and ethanol are viable substitutes to limit the decline of this resource due to their similar physical characteristics. They could provide a long-term vehicle power solution. Combustion of these two fuels has also been widely documented to reduce harmful emissions, such as $CO_2$, $NO_x$ and CO, that pose long-term risks to the environment's condition. The following equations show the reaction for each fuel alongside the enthalpy of combustion (heating value). As gasoline is a mixture of hydrocarbons, it is standard procedure to approximate as octane, which can be seen below:

$$\text{Octane}: \quad C_8H_{18} + 12.5O_2 \rightarrow 8CO_2 + 9H_2O \ \ (-47.87\ \text{kJ/g}) \tag{1}$$

$$\text{Methanol}: \quad CH_3OH + 1.5O_2 \rightarrow CO_2 + 2H_2O \ \ (-22.65\ \text{kJ/g}) \tag{2}$$

$$\text{Ethanol}: \quad C_2H_5OH + 3O_2 \rightarrow 2CO_2 + 3H_2O \ \ (-29.67\ \text{kJ/g}) \tag{3}$$

Evidently, 8 times more $CO_2$ is produced by gasoline per molecule than methanol and 4 times more than ethanol. As seen, methanol and ethanol produce 47.3% and 62.0% of gasoline's energy per gram combusted, respectively, and therefore more biofuel must be combusted for equivalent power outputs and thus a larger BSFC is expected. Qi [14] confirmed this theory due also to lower stoichiometric air fuel ratios. The specific energy consumption however was found by Qi to be 1.8% lower for M10 (10% methanol, 90% gasoline) and 3.6% lower for M25. This is due to an increase in volumetric efficiency with increased fraction [14]. Using Equations (1)–(3), for a standardised amount of energy production, molecules of $CO_2$ emitted are distributed in the ratio gasoline:methanol:ethanol as 80:21:32. Therefore, despite the added fuel consumption for the biofuels, the $CO_2$ emission savings are still significant.

A major benefit of alcohol introduction is an increased brake thermal efficiency and brake power output for certain mass fractions. Iliev's 2014 study [21] showed that low alcohol fractions instigated increased power output, as the added oxygen content provided increased combustion efficiency. Elfasakhany [22] showed this efficiency increase to also be due to the increased latent heat of vaporisation for each alcohol, 2.7 times for ethanol and 3.6 times for methanol. This caused a decreased intake manifold temperature and thus improved combustion conditions [22]. Large mass fractions of alcohols however cause the overall heating value of the blend to be reduced. As this becomes the dominant factor, power output at all loads is reduced. As observed by Qi [14], maximum power dropped by 2.3% and 6.8%, with M10 and M25, respectively. Reduced heating values also instigate less heat production. As such, peak combustion temperature and charge temperature following compression are reduced. This mitigates $NO_x$'s three production methods: thermal $NO_x$, fuel $NO_x$ and prompt $NO_x$ [3]. Alcohols also do not contain nitrogen, further limiting fuel NOx production.

CO and HC production can also be heavily reduced. The added oxygenates provide favourable conditions, and as such limit CO and HC's primary method of formation, incomplete combustion. Qi [14] reported a 73% and 53% reduction in CO emissions with M10 and M25 blends at medium load, respectively. In terms of HC, it has been found that the major areas of formation are crevices in the cylinder walls that prevent oxidation [23]. The reduced quenching distance of both methanol and ethanol allow for the combustion flame to propagate into these crevices and instigate further combustion. The reduction

of cylinder temperature may also reduce the formation of CO by dissociation [24]. If the cylinder temperature becomes too low however incomplete combustion may again be a concern. Furthermore, a concern is the significant increase in BSFC; this increased fuel volume will reduce the air–fuel ratio within the cylinder and therefore promote HC output through unburned fuel content. Evidence for this was presented by Qi [14], who reported a 50% reduction of HC emissions with M10, but a 1400% increase for M25 at medium load.

### *2.3. Model Creation Method*

To realise these numerical investigations as physical developments, the first key step was to produce a 1D model accurately representing a production engine. This was carried out within Ricardo's 1D gas dynamics tool 'WAVE', a 1D Navier–Stokes equation solver. 'WAVE' utilises the Navier–Stokes equations governing the transfer of mass, momentum and energy for compressible gas flows. These are solved based upon the physical information input by the user in the form of a model, in this case Figure 2. Physical inputs such as cylinder count and dimensions will impact the output of the Navier–Stokes equations and thus the mechanical performance of the engine. 'WAVE' also contains submodels to determine the behaviour and output of both combustion and emissions, governed by further equations, NOx emissions for example are defined by the Arrhenius equation for the kinetic rates. The Multi–Wiebe combustion model was in this case utilised due to the dual-fuel nature of the investigation. Investigations were based on an engine whose physical construction was based upon the 1D model, comprised of components (cylinders, etc.) within 'WAVE' with properties set to match the physical specification. Ricardo's engine database contains several solutions from which the McLaren M838T was chosen. This decision was made due to the scarcity of literature investigating the reduction of the environmental impact of 'sports' cars, of which energy recovery systems dominate the market. Significant modifications were made for compatibility with the concerns of this work alongside a rebuild of the model to better understand the intentions of the original engineers.

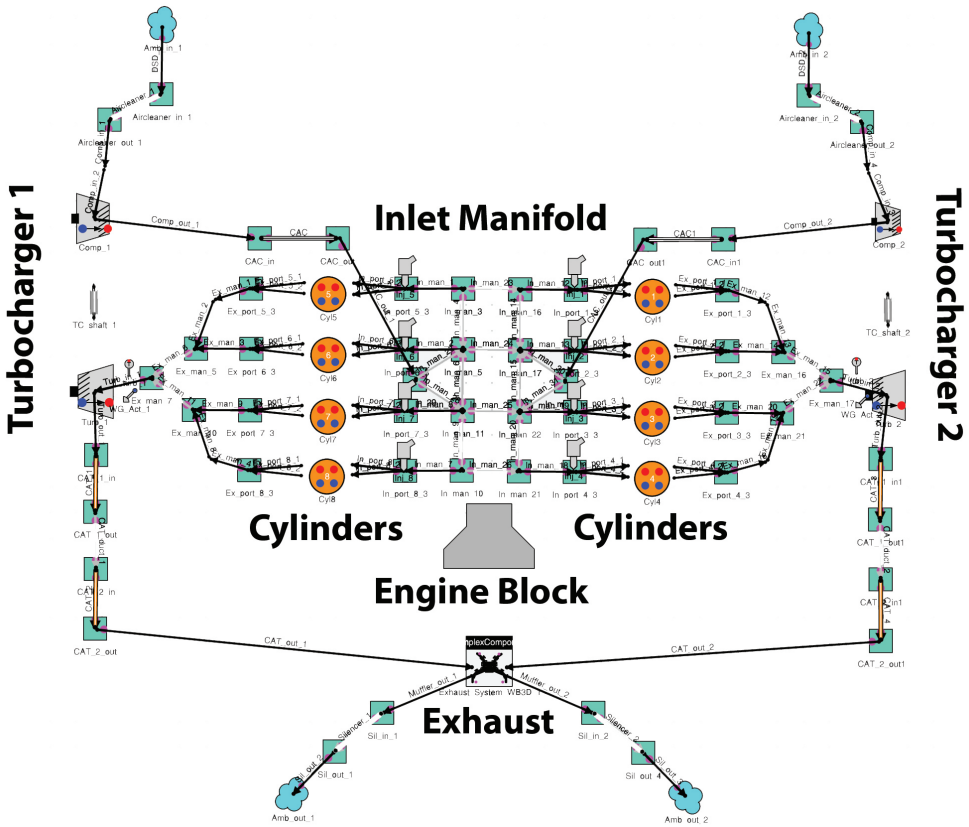


**Figure 2.** Baseline 1D CFD M838T engine model.

### *2.4. Emission Model Application*

Both the spark ignition (SI) and direct injection (DI) HC emission models were integrated within the engine and activated. The post-flame oxidation behaviour was also activated for fully accurate HC outputs. $NO_x$ and CO emission models required activation, as well as assigning them a passive scalar. The passive scalars were created such that the simulation could track the quantity of substances of specific molecular weight, in this case the targeted emissions.

### *2.5. Modified Fuel Application*

A variety of methanol and ethanol blends were required for application to the engine for investigation. The 'Buildfuel' application within WAVE was used for this, accessed and manipulated through the command prompt. Each fuel blend was implemented within the model properties and fuel injection was left on proportional for automatic fuel/air ratio correction. For the baseline model a 100% gasoline fuel was created. Each fuel blend created was then applied to the baseline system.

### *2.6. Miller Cycle Application*

The baseline profile was extracted first and using values within this profile both the EIVC and LIVC profiles were modelled. The exhaust valve profile was not altered within this investigation and as such the valve overlap angle was consistent for all examples. Profile shapes were constructed based upon definitions by Wei [25]. These profiles are presented in Figure 3, where EIVC 30 defines a profile in which the valve closes 30 degrees earlier than the baseline profile.

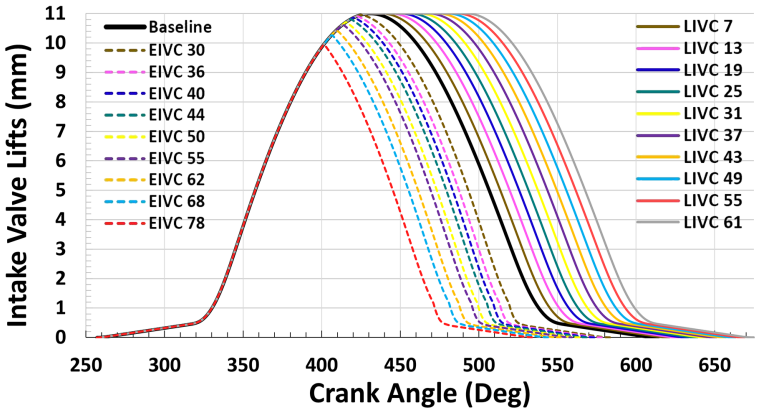


**Figure 3.** Investigated Miller cycle intake valve profiles.

### *2.7. Engine Model Performance Validation*

The physical M838T was constructed based on the 1D model used within this investigation and it was therefore expected that the model would be an accurate representation of the physical engine. Following the manual changes made however, validation was required to confirm that changes did not affect its base characteristics. Due to limited published data, dynanometer values [26] were compared to the model outputs in Figure 4.

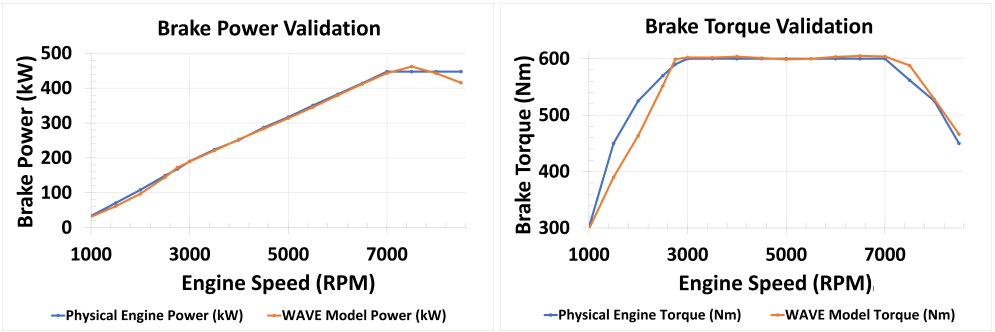


(**a**) (**b**)

**Figure 4.** Engine performance validation. (**a**) Power Comparison; (**b**) Torque Comparison.

The model followed the physical engine characteristics very closely, with only slight variations in the overall pattern at extreme load conditions. To confirm validation, the majority of points must lie within 5% of the dynanometer values, providing an indication of a successful model. Table 1 presents the percentage differences at each engine load. Few large deviations occur at over-speeding and very low load that exceed the 5% threshold. Due to the unpredictability of performance within these regions the model can be considered valid for mechanical output, as it satisfied the bulk operation conditions.

**Table 1.** 1D model performance percentage differences.

| **Speed (RPM)** | 8500 | 8000 | 7500 | 7000 | 6500 | 6000 |
|---|---|---|---|---|---|---|
| **Power PD (%)** | −7.21 | −1.10 | 3.23 | −1.02 | −0.48 | −0.80 |
| **Torque PD (%)** | 3.64 | 0.61 | 4.64 | 0.69 | 0.85 | 0.56 |
| **Speed (RPM)** | 5500 | 5000 | 4500 | 4000 | 3500 | 3000 |
| **Power PD (%)** | −1.38 | −1.05 | −1.30 | 0.50 | −1.36 | −0.51 |
| **Torque PD (%)** | 0.023 | −0.18 | 0.22 | 0.64 | 0.34 | 0.37 |
| **Speed (RPM)** | 2750 | 2500 | 2000 | 1500 | 1000 | |
| **Power PD (%)** | 2.84 | −3.0 | −10.25 | −13.49 | −7.27 | |
| **Torque PD (%)** | 1.56 | −3.14 | −11.74 | −13.30 | −0.95 | |

### *2.8. Emission Model Validation*

To determine if the emission behaviours shown by the engine were an accurate representation of real outputs, a further verification step was required. Due to the extremely limited emission data surrounding the M838T, an indirect method was used. A similar preset engine (2.2 L twin-turbo gasoline) was taken from Ricardo's database and simulated as a comparison. The emission levels were plotted as standardised amounts per engine litre and each engine compared in Figure 5. As these engines intrinsically differ from each other, this process tested overall trends as opposed to specific point differences. Each overall trend was matched. Despite standardisation, however, some obvious discrepancies were observed, particularly for the HC emissions which showed a consistent shift in all results. This is to be expected however as varying engine sizes differ with a non-linear relationship to fuel consumption. For both $NO_x$ and CO emissions, strong correlation can be seen at high engine load, with only relatively large differences at low load. However, again, due to the unpredictability of engine behaviour at low load, these differences are not significant. The majority of points of difference were below 10%; therefore, the engine for both mechanical and emission outputs was successfully validated.

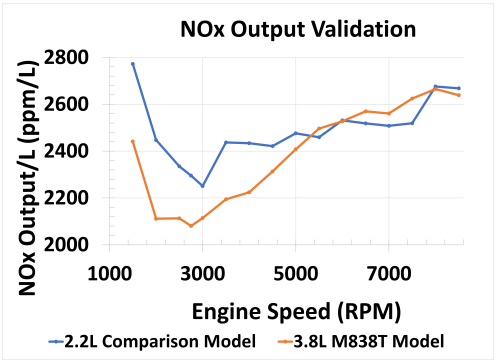


(**a**)

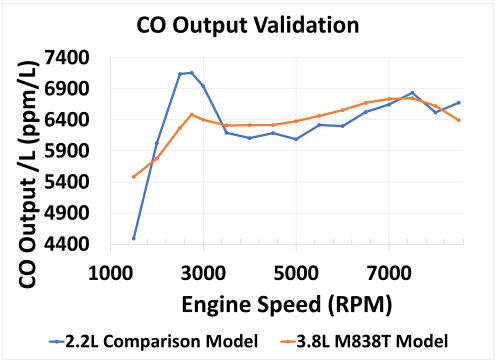


(**b**)

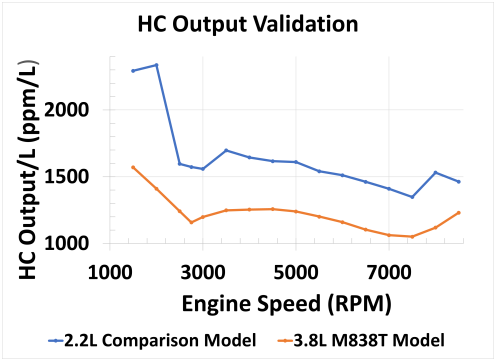


(**c**)

| Engine Speed (RPM) | Percentage Difference (%) | | |
|---|---|---|---|
| | NOx | CO | HC |
| 2000 | −13.4 | −4.1 | −42.9 |
| 3000 | −5.8 | −7.5 | −22.6 |
| 4000 | −8.5 | −3.7 | −24.5 |
| 5000 | −3.2 | 4.6 | −21.9 |
| 6000 | −0.1 | −4.0 | −21.3 |
| 7000 | 1.6 | 0.8 | −25.0 |
| 8000 | 0.2 | 1.9 | −26.0 |

(**d**)

**Figure 5.** Engine emission validation. (**a**) $NO_x$ Comparison; (**b**) CO Comparison; (**c**) HC Comparison; (**d**) Percentage Differences.

## 3. Results and Discussion

Within this section the outputs of all simulations have been documented and discussed. The EIVC and LIVC Miller cycles were investigated across varying magnitudes of closure. Within this section, EIVC30, for example, denotes an early intake valve close implementation that closes 30 degrees earlier than the baseline profile. Outputs of varying mass fraction blends of gasoline have also been presented. In this case M30, for example, denotes a fuel blend consisting of 30% methanol and 70% gasoline. Alternatively E has been used to denote an ethanol mix. Within this section outputs from varying airflow through the two turbochargers have been presented as well simulations combining multiple of the above technologies. All properties of concern, both mechanical and emission outputs have been graphed across all engine loads.

### *3.1. Methanol Blends*

#### 3.1.1. Engine Performance

Figure 6 presents the performance results for varying mass fractions of methanol with gasoline. Blends up to M40 lost approximately 18.4 kW brake power at peak for each increase in 10% of methanol. M40 and above suffered an excess of 30 kW loss for the same increase. The M5 blend achieved a marginal 0.15 kW increase between 1000 RPM and 1858 RPM. In this period, the added oxygen was dominant over the limiting heating value, supporting Iliev's findings [21]. Each addition of 10% of methanol saw a rough increase of 0.5% efficiency at peak. This effect was reduced both above and below this engine load. High fraction blends saw large drop offs in efficiency at high loads, due to the increased flame propagation speed decreasing combustion time. The increased resistive pressure prior to TDC, worked against the piston (This is elaborated on in Section 3.3.) As combustion time decreased at high load, the positive pressure effect post TDC was reduced and resistive pressure was dominant in reducing performance [20]. The BSFC increased

exponentially with increasing mass fraction, a phenomenon documented by Qi [14]. M100 showed a minimum 100% increase on the baseline. The exponential increase is likely due to a greatly reduced air–fuel ratio, due to large fuel volumes entering the cylinder. This reduced complete combustion rates due to limited oxygen availability.

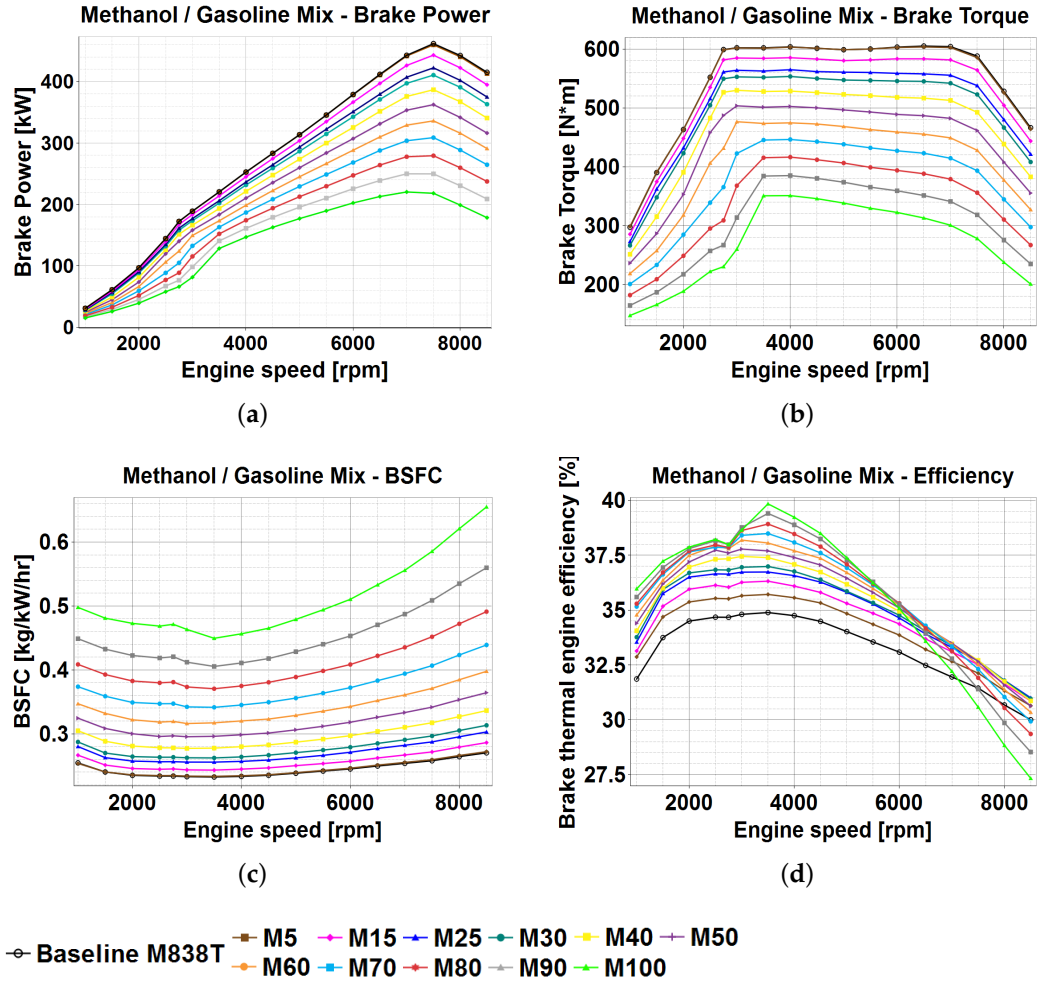


**Figure 6.** Methanol and gasoline blends: engine performance outputs. (**a**) Brake Power; (**b**) Brake Torque; (**c**) BSFC; (**d**) Brake Thermal Efficiency.

### 3.1.2. Emissions

Figure 7 presents the emission outputs of varying mass fractions of methanol with gasoline. All blends, excluding M5 and M15, caused an overall reduction in $NO_x$ emissions. Iliev [21] described an increase for all blends up to M50 due to increased cylinder temperature. The dominant factor for M5 and M15 was therefore the flame propagation speed as power and temperature output was reduced for both, which for methanol is 63 cm/s compared to 52 cm/s for gasoline [27], causing increased levels of $NO_x$, as suggested by Larfeldt [28]. M100 ultimately caused a 99% reduction in NOx ouput at rated speed due to reduced combustion temperatures. Reductions in CO output for all blends were also observed due to the introduction of added oxygen and reduced carbon chains. The promising M30 caused a 91.4% reduction, confirming findings by Qi [14]. Mass fractions up to M40 showed a complex HC pattern across engine loads, with an overall decrease with increasing load. This pattern is not seen in most studies, which tend to show a roughly linear decrease. Complexities were due to localised efficiency/temperature variations. The initial decrease corresponds to the increasing engine efficiency and reduction of BSFC, to the point of highest efficiency at 2750 RPM. The following increase is due to the correspond-

ing decrease in engine efficiency and increase in unburned fuel. This continues up until approximately 4500 RPM, when cylinder temperature begins to dominate as the engine's output power continues to increase. HC output then decreases roughly linearly to a minimum at rated speed. The HC increase at speeds exceeding the rated speed correspond to extreme fuel-rich conditions. Combustion rates decreased due to the smaller combustion time and oxygen availability, and therefore more unburned fuel (HC) was output. M50 and above blends showed a slight difference: an increasing trend between 1000 RPM and 2750 RPM, due to the exponentially increased BSFC and low air–fuel ratio. The M5 blend showed a decrease in HC output from the baseline at all engine speeds. This supports Zhao's findings [29], and is due to the added oxygenate promoting complete combustion. In addition the methanol has a shorter quenching distance, meaning the combustion flame could form closer to the cylinder wall, allowing complete combustion at the main formation point [23]. From M15 to M60, increasing methanol fraction increased HC output. This was due to increased unburned fuel from the increased fuel-air ratio. From M60 to M100 however, a reduction in HC output is seen; this change in pattern occurs as methanol becomes the majority fuel. It is likely the shorter hydrocarbon chains, alongside the shorter quenching distance and added oxygenation dominated the reduced cylinder temperature.

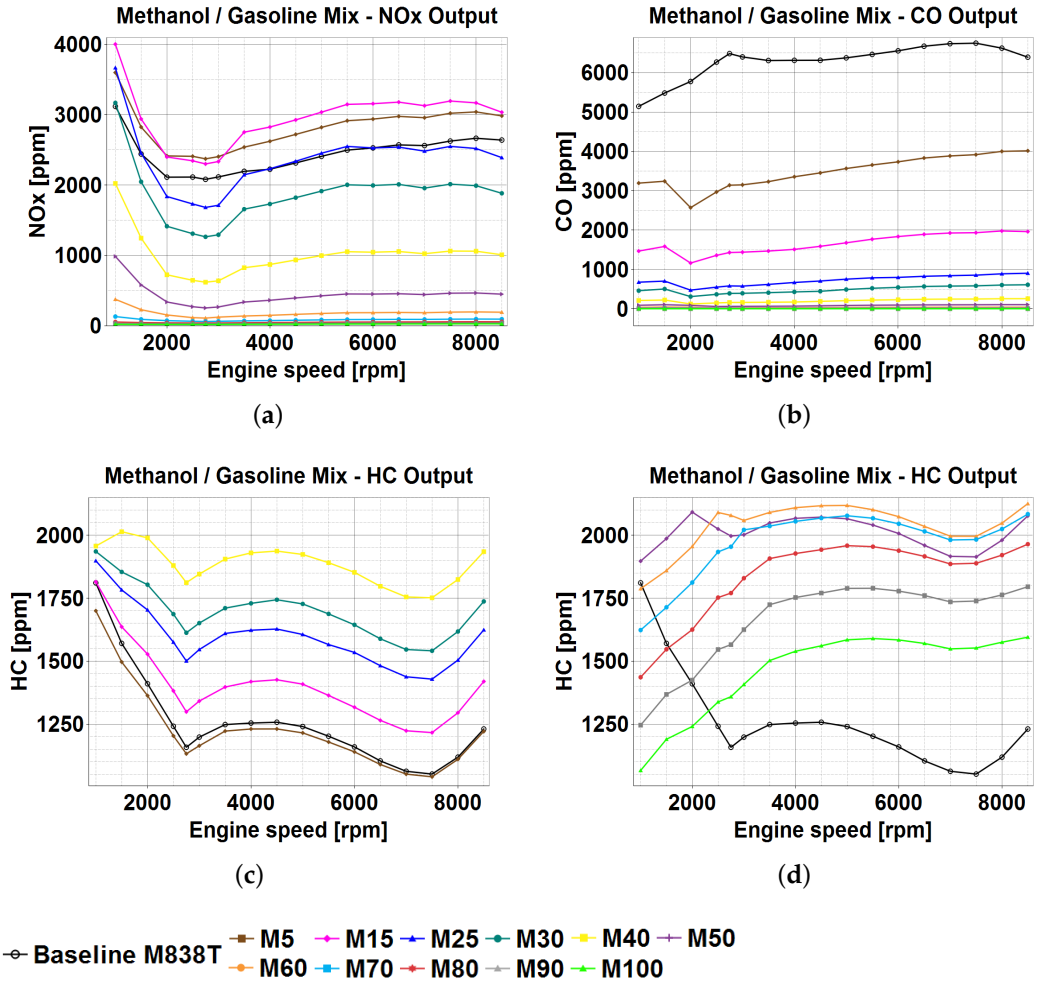


**Figure 7.** Methanol and gasoline blends: emission outputs. (**a**) $NO_x$; (**b**) CO; (**c**) HC (M5–M40); (**d**) HC (M50–M100).

### *3.2. Ethanol Blends*

#### 3.2.1. Engine Performance

Figure 8 presents the performance results for varying mass fractions of ethanol with gasoline. Similar trends to that of methanol were observed across all parameters, due to little variation in the two fuels' intrinsic properties. As such, the reasoning behind improvements/drawbacks are identical unless stated otherwise. The E5 blend achieved a 9.3 kW brake power upgrade across all loads below 8350 RPM. The increase on M5 was due to the larger heating value. For large mass fractions, the reduced heating value caused a 17.2 kW brake power drop for every 10% ethanol increase. Again, the BSFC increased exponentially as ethanol fraction increased. Ethanol did however show a less extreme increase than methanol, which showed a BSFC of 0.5855 kg/kwh at rated speed compared to 0.417 kg/kwh for 100% blends. Ethanol also showed a significant efficiency increase for all blends, E5 achieved a 0.72% efficiency increase to 35.6% at peak. E100 also achieved an increase of 3.66% to 38.55% at peak. E5 at peak was lower than M5 by 0.1% and E100 to M100 by 1.28%.

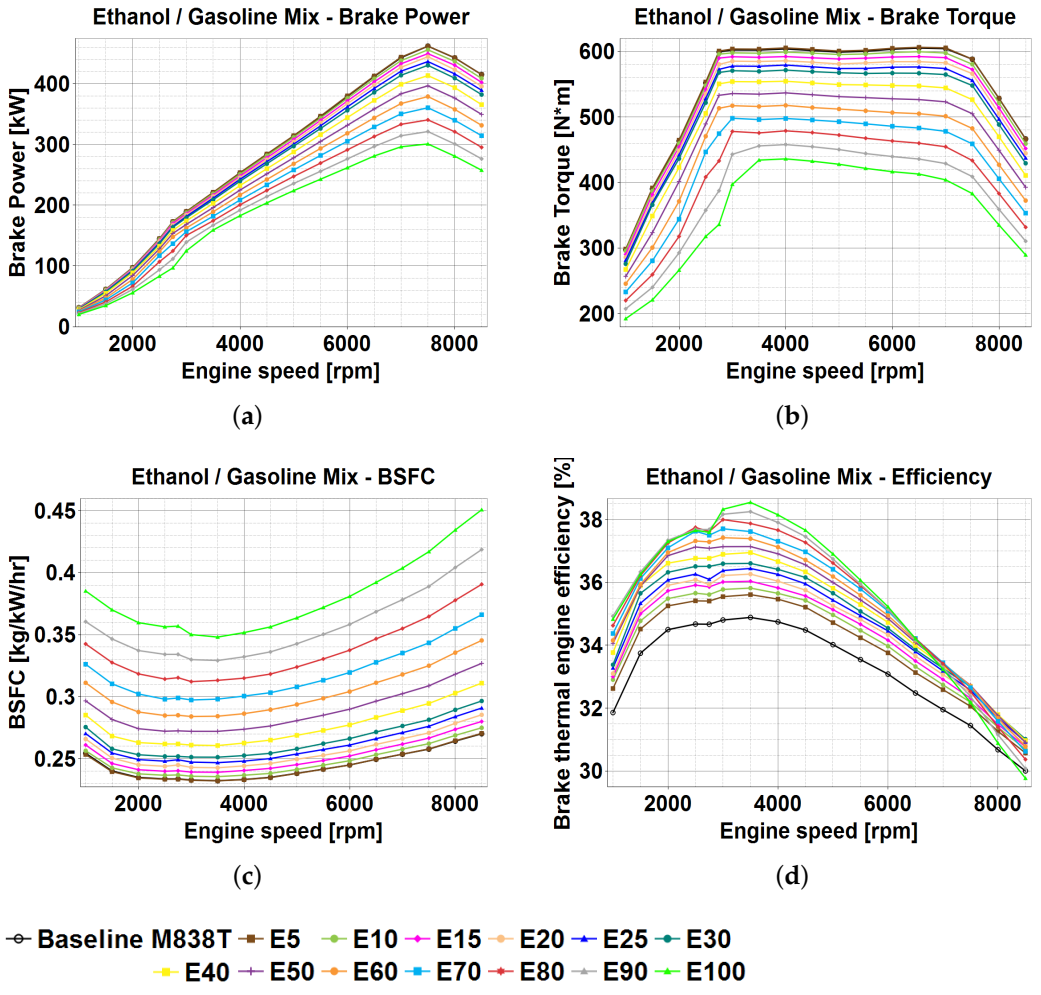


**Figure 8.** Ethanol and gasoline blends: engine performance outputs. (**a**) Brake Power; (**b**) Brake Torque; (**c**) BSFC; (**d**) Brake Thermal Efficiency.

#### 3.2.2. Emissions

Figure 9 presents the emission outputs of varying mass fractions of ethanol with gasoline. Ethanol blends of E30 and lower caused increased $NO_x$ output. This has been detailed by past reports [30] and was due to increased cylinder temperature during combustion. Figure 9d shows the increase of cylinder temperature during the 4-stroke cycle

for E5. E15 however contradicts this. As for methanol, the dominant factor was therefore assumed to be flame propagation speed for E10 to E30 blends, causing increased levels of $NO_x$, as power output was reduced for these blends [28,29]. E40 and larger blends saw significant reductions in $NO_x$ emissions due to the lowered cylinder temperature caused by the decreasing heating value. CO emissions decreased with increasing ethanol fraction, again due to the added oxygenation provided by the biofuel instigating further complete combustion [14]. A similar pattern to methanol is seen for HC output. In this case, however, the trend switch occurs for fractions of E60 and larger, where an increase is seen at low engine load. This is again due to the larger BSFC caused by reduced heating value. Seen also in this figure is the reduction of HC output for E5, 3% at rated speed, due to increased combustion temperature and added oxygenates.

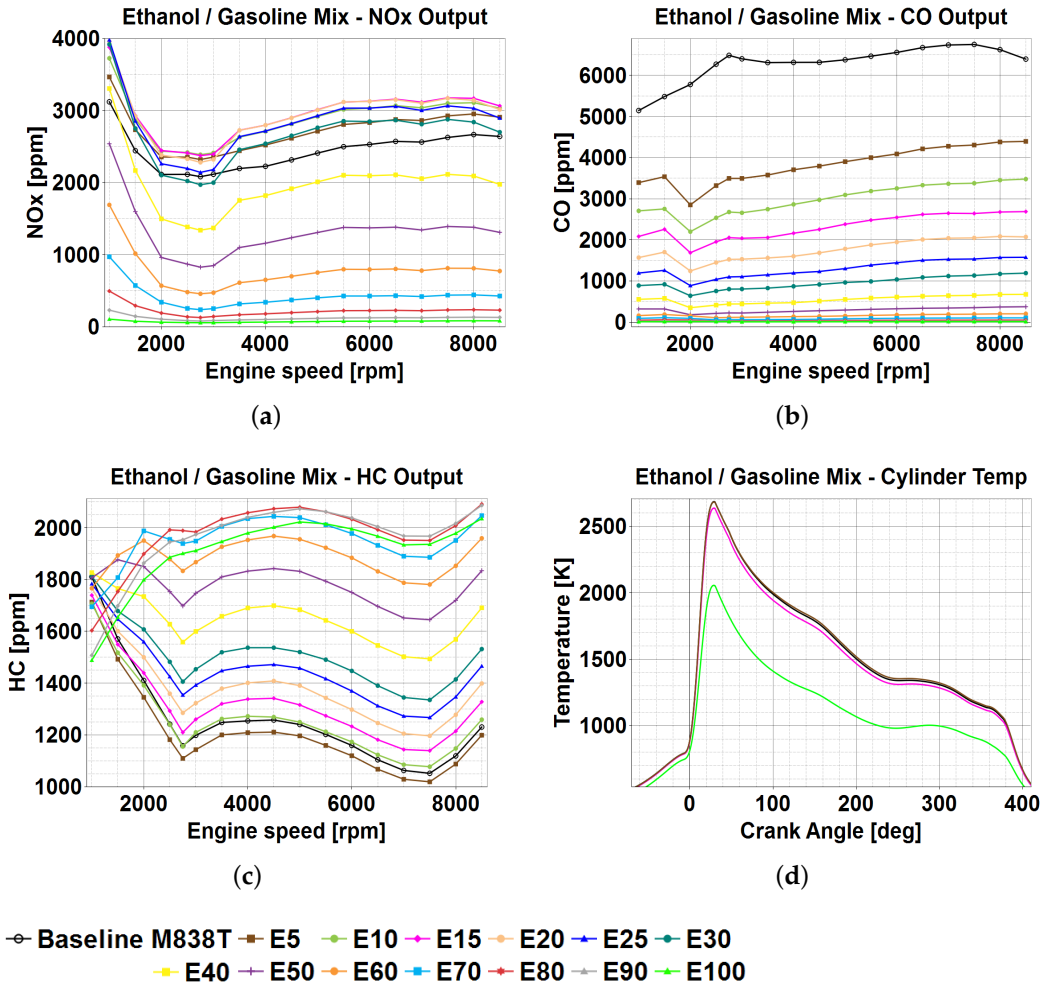


**Figure 9.** Ethanol and gasoline blends: emission outputs. (**a**) $NO_x$; (**b**) CO; (**c**) HC; (**d**) Temperature Comparison.

### *3.3. Biofuel and Gasoline 100% Fraction Comparison*

Figures 6a and 8a confirmed feasible usage of 100% mass fraction biofuels within the M838T. Methanol provided superior thermal efficiency, by 1.4% and HC reduction by 26%. Efficiency differences were due to increased latent heat of vaporisation and octane numbers. The octane numbers of which are 119 for methanol, 113 for ethanol and 87 for gasoline. This resistance to compression has been attributed to increased efficiency [31]. This may also explain potential increases in performance when used with the EIVC. Ethanol instead achieved higher power output, by 27%, and improved BSFC by 38%, seen below in Figure 10a,c. These figures present a mechanical output comparison of operation with 100%

mass fraction of each fuel type. Figure 10b,d shows in-cylinder temperatures and pressures, respectively, of the two biofuels during combustion, illustrating discussions in Sections 3.1 and 3.2. Furthermore, the feasibility of exclusive operation is highlighted, which is possible with significant performance loss. Shown in Figure 10c is the significant increase of BSFC for the M100 blend at high load. As discussed, this is due to the large volumes of fuel in the cylinder, prompting high fuel-air ratios. The significant efficiency loss for M100 and E100 was highlighted in Figures 6d and 8d so is not included here. This was due to high fuel-air ratios and reduced combustion time, limiting the impact of positive post-TDC pressure. Note that M100 becomes less efficient than E100 at speeds exceeding 5750 RPM.

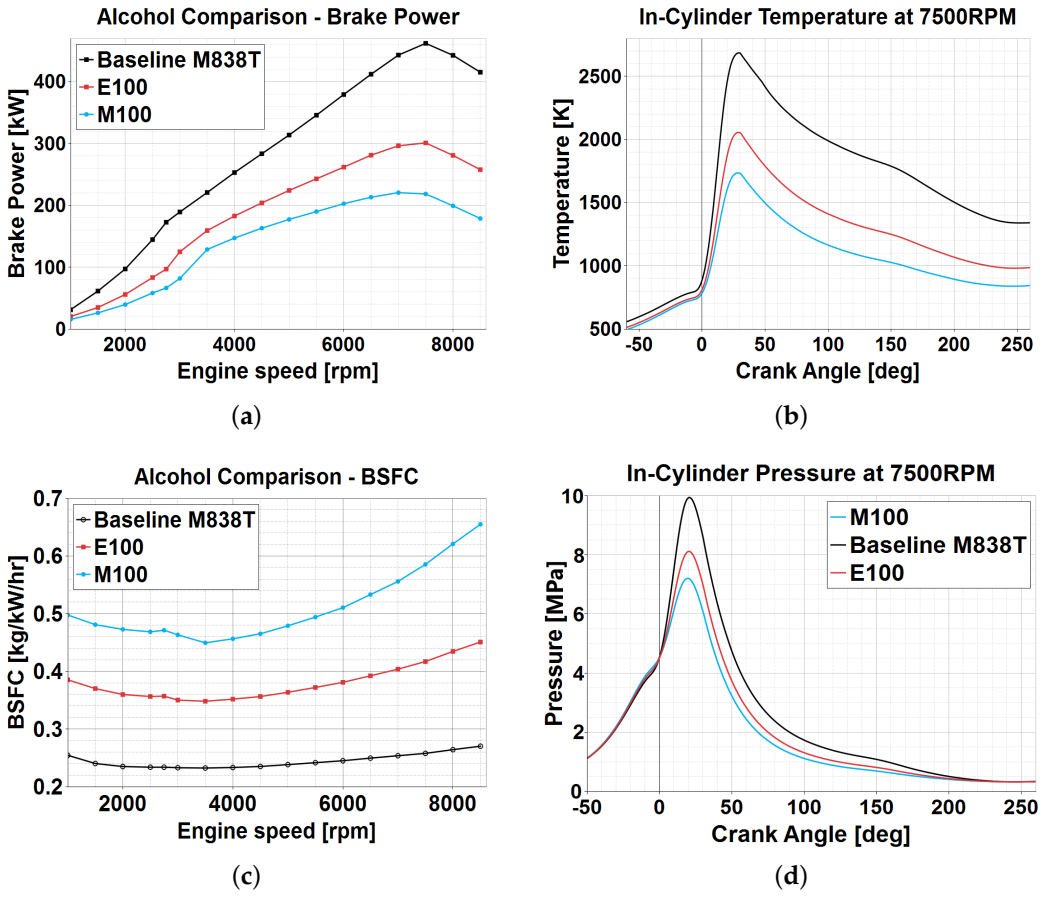


**Figure 10.** Biofuel combustion comparison. (**a**) Power Output; (**b**) Temperature; (**c**) Brake Specific Fuel Consumption; (**d**) Pressure.

### *3.4. Early Intake Valve Close*

#### 3.4.1. Engine Performance

Following the application of the EIVC valve lift profiles seen in Figure 3, Figure 11 shows the corresponding performance outputs. Power output increased for all applications at low and medium load. For the 30 degree early close, a 19.3 kW (7%) power increase acts up to 6750 RPM. The power increase varied little between magnitudes of early closure, 50 degree EIVC shows the largest increase of 26.8 kW (9.5%). An increase in cylinder pressure was observed. This was due to the reduction of in-cylinder combustion duration stemmed from the earlier valve close [10]. This has been elaborated on in Section 3.7. This directly reduces pumping losses and thus promotes increased cycle performance [10,32]. Power loss was observed at high engine load, Huang [9] observed this in a similar specification engine in 2020. They reasoned that the reduction of air intake due to the EIVC severely limited engine performance in demanding conditions. A large increase in pressure for the EIVC prior to TDC was found at 0 degrees. This pressure works against piston

rising and becomes more prominent at higher load, as combustion time is reduced and positive pressure post TDC is reduced [20]. This has again been elaborated on in Section 3.7. Application of the Miller cycle at very high loads, in high-performance vehicles, is not well documented in literature. These results therefore show a gap in research and build upon expected results. Both BSFC and thermal efficiency show marginal improvements across both low and medium engine loads; a common finding across similar research. This is due to the decoupled expansion ratio, allowing more work to be extracted from the cycle. This is an idea heavily documented by Tengku [33]. The reduction of pumping losses following EIVC application contributes to an efficiency increase [10], a direct consequence of the increased cylinder pressure.

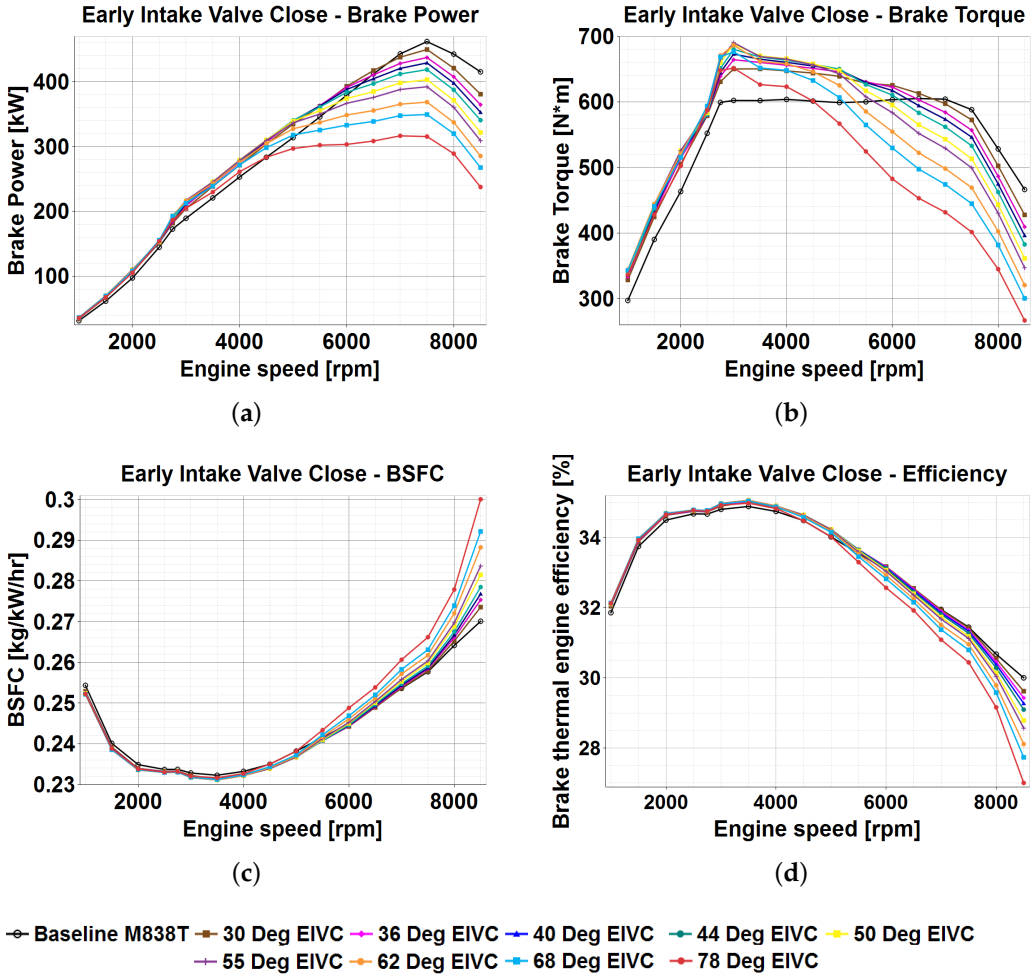


**Figure 11.** Early intake valve close Miller cycles: engine performance outputs. (**a**) Brake Power; (**b**) Brake Torque; (**c**) BSFC; (**d**) Brake Thermal Efficiency.

### 3.4.2. Emissions

Following the application of the EIVC valve lift profiles seen in Figure 3, Figure 12 shows the corresponding emission outputs. The increased cylinder temperature resulted in increased $NO_x$ output at low and medium loads. The 30-degree EIVC profile resulted in a 2.2% increase, with reductions at loads greater than 6500 RPM. As discussed in Section 3.7. At rated speed, a reduction of 2.3% was observed. For the final combined solutions, the alcohol will be the dominant factor in $NO_x$ emissions and as such marginal increases are acceptable for the Miller cycle. Most profiles resulted in an increase in CO output at low and medium engine loads. There is a net reduction in air intake for the EIVC as stated by Wang [11]. This likely leads to the increase in CO emissions at low load due to the lack

of available oxygen. The decrease therefore at higher loads will be due to the increased temperature driving further complete combustion. EIVC achieved HC reductions at both low and medium loads. These reductions, as for the BSFC, are due to the increase in work extracted from the cycle. The reduced pumping losses allow for increased fuel utilisation and thus less fuel is output as unburned hydrocarbons. In terms of this investigation this has high potential for operation alongside the biofuels, the main negative of which is HC output increase.

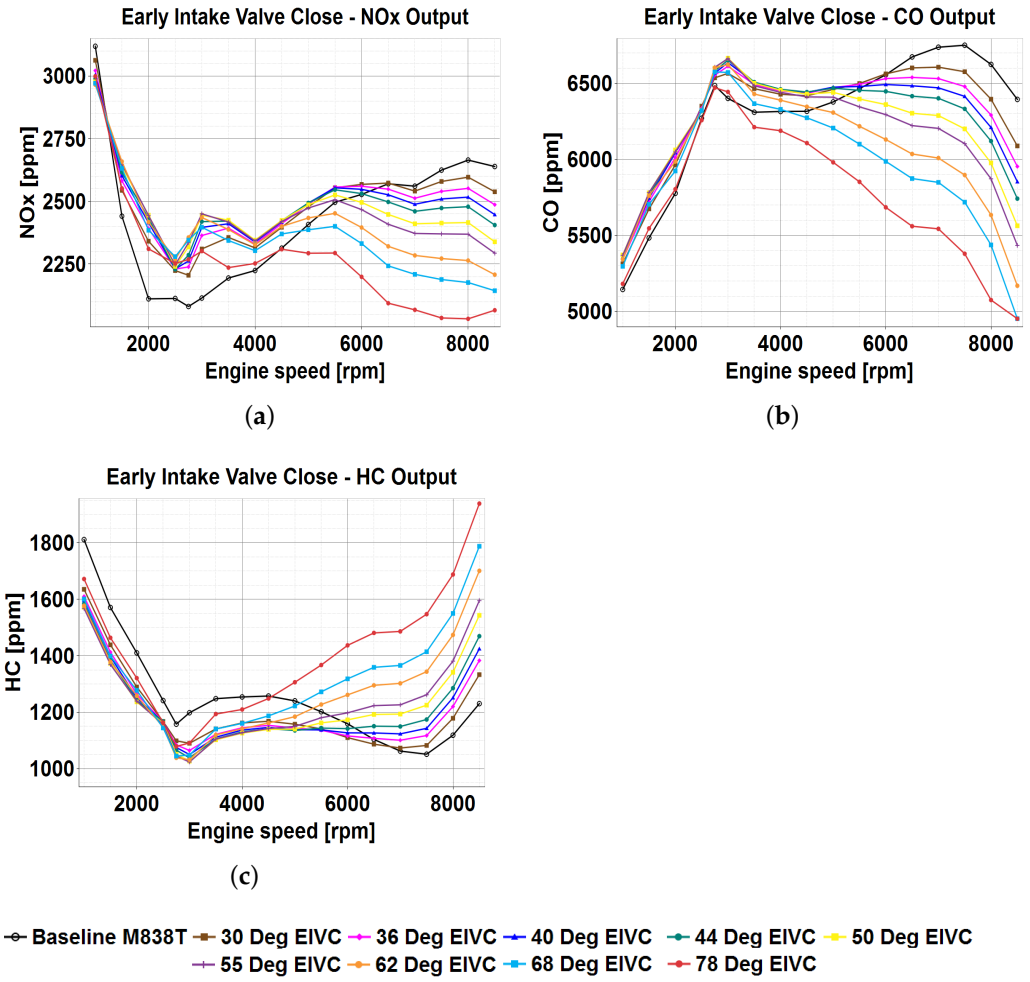


**Figure 12.** Early intake valve close Miller cycles: emission outputs. (**a**) $NO_x$; (**b**) CO; (**c**) HC.

### *3.5. Late Intake Valve Close*

#### 3.5.1. Engine Performance

Following the application of the LIVC valve lift profiles seen in Figure 3, Figure 13 shows the corresponding performance outputs. A reduction in power output at all engine loads was observed. This was due to the loss of charge during the blow-back period [8] and the significant loss in cylinder pressure. The 31-degree LIVC shows a power loss of 40 kW at peak. At very high load only marginal power loss was observed however, unlike the baseline. This is likely due to the reduced combustion duration at high load compensating for charge lost during blow-back. A negative effect on both BSFC and thermal efficiency can be observed for all engine loads. It was anticipated that the reduced inlet charge temperature and increased work extracted from the cycle would improve efficiency, however the loss of charge during blow-back and reduced combustion temperature and pressure have been dominant in reducing energy extraction. Thirty-one-degree LIVC caused an increased BSFC at rated speed of 1% and an efficiency reduction of 1.1%.

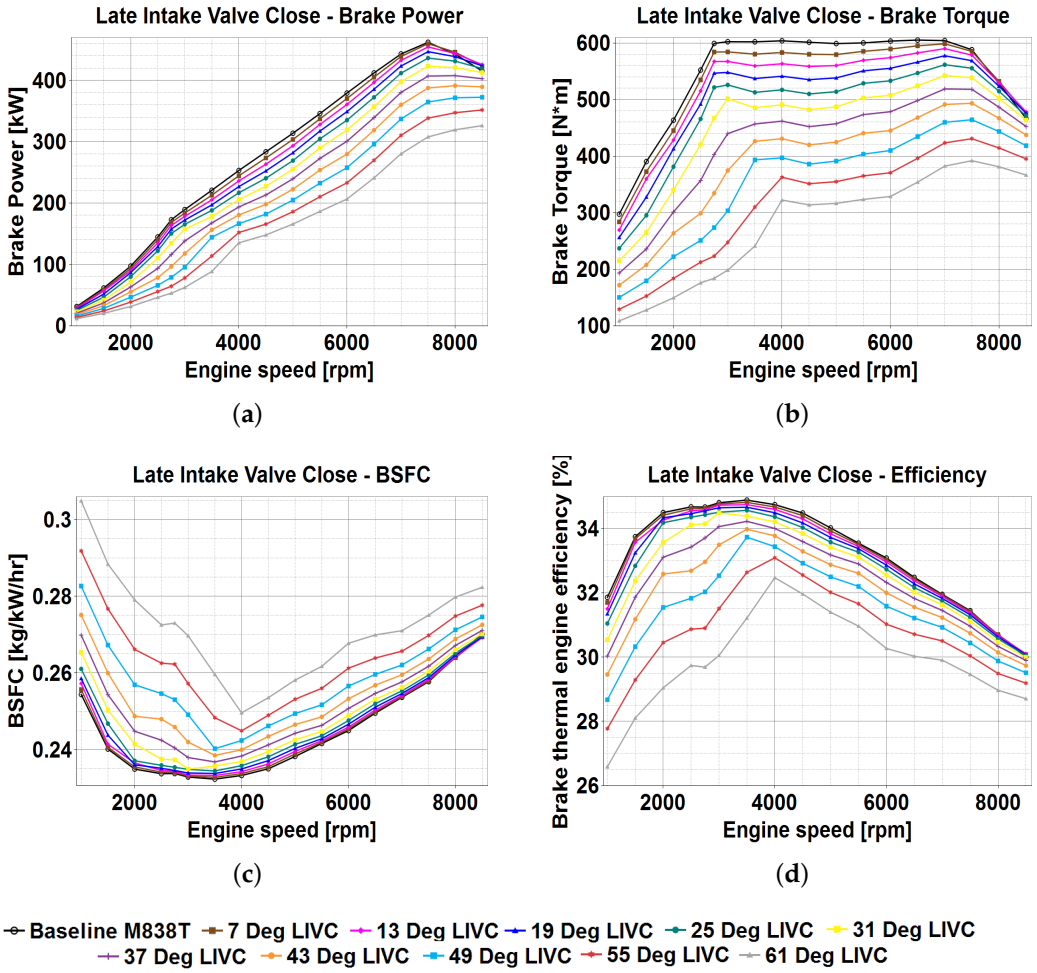


**Figure 13.** Late intake valve close Miller cycles: engine performance and emission outputs. (**a**) Brake Power; (**b**) Brake Torque; (**c**) BSFC; (**d**) Brake Thermal Efficiency.

### 3.5.2. Emissions

Following the application of the LIVC valve lift profiles seen in Figure 3, Figure 14 shows the corresponding emission outputs. Figure 14a,b shows a reduction of $NO_x$ and CO emissions across all loads for small LIVC. $NO_x$ emission reduction was due to reduced charge and peak cylinder temperatures. As elaborated on in Section 3.7. Thirty-one-deg LIVC achieved $NO_x$ reductions of 10% through mid loads and 3% at rated speed. As well as CO reductions of 8% at mid load and 1% at rated speed. He [34] stated that CO reduction was attributed to the reduced frequency of localised fuel-rich combustion zones. The zones limited complete combustion frequency due to oxygen deficiency. This impact became less prominent at high load as fuel consumption increased alongside increased localised fuel-rich zones. This was no longer observed for LIVC of 37 degrees or more as the limited cylinder temperature inhibited complete combustion. HC emissions saw an incremental increase as LIVC became larger, corresponding to that of the BSFC increase. Both factors are direct result of the unburned fuel expelled from the cylinder during the blow-back period. HC output became less impacted at high load due to both increased cylinder temperature and reduced combustion time limiting the mass of fuel lost.

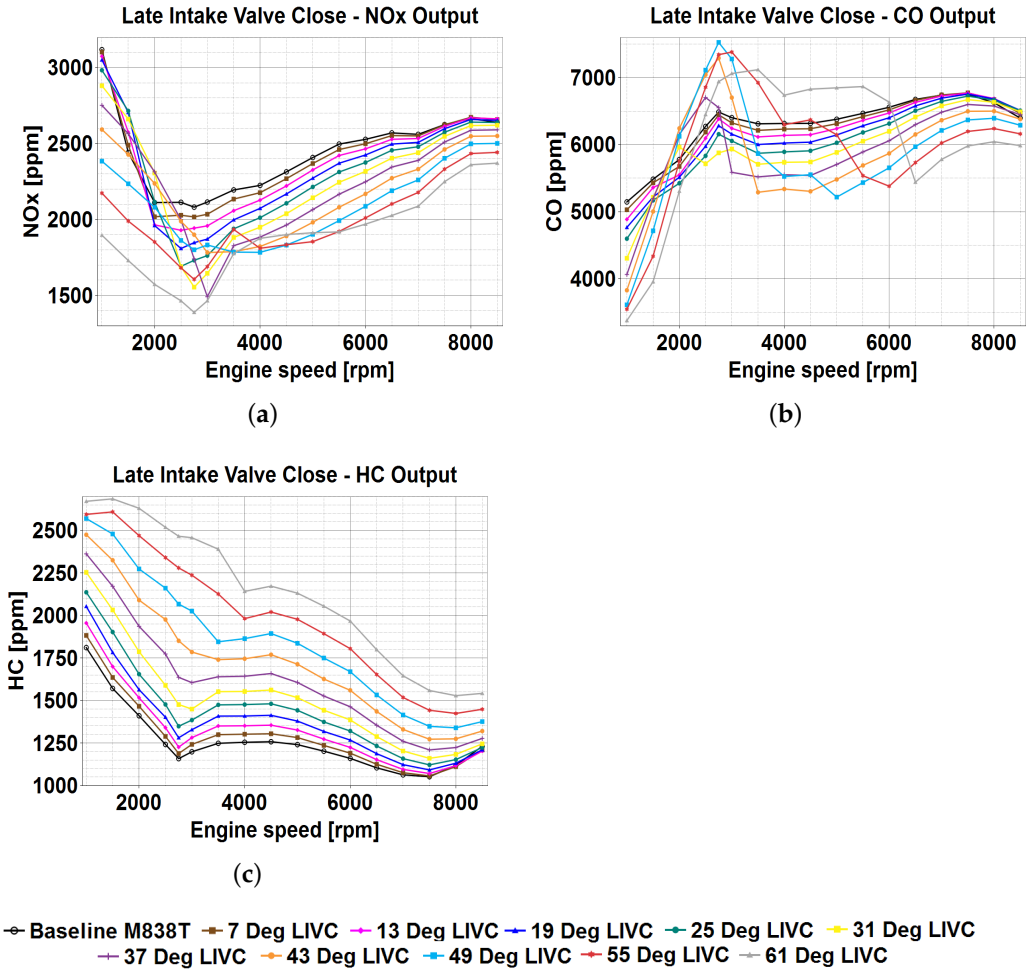


**Figure 14.** Late intake valve close Miller cycles: engine performance and emission outputs. (**a**) $NO_x$; (**b**) CO; (**c**) HC.

### *3.6. Turbocharger Variation*

Air mass flow was varied on the twin-turbo system to understand the effects on performance and emissions, outputs from this are seen in Figures 15–17. The M30 blend was chosen as a basis for investigation. As can be seen in Figure 15a power compensation at high load was achieved for all mass flow increases.

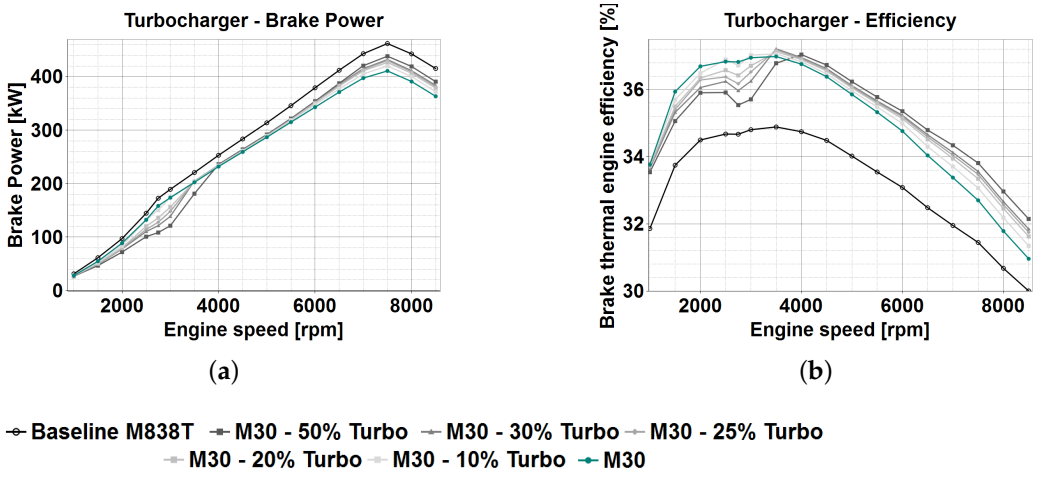


**Figure 15.** Varied turbocharger outputs. (**a**) Brake Power; (**b**) Brake Thermal Efficiency.

Fifty percent mass flow increase saw an improvement of 28.1 kW (6.86%), due to the added oxygen instigating further combustion in oxygen demanding conditions. Mass flow was also varied to compensate for loss of charge during the Miller cycle, as detailed in Section 3.8. Loads below 3000 RPM saw power loss for all mass flows, again seen in Figure 15a; the added air caused an excessive air–fuel ratio, resulting in an exceedingly lean charge mixture and limited flame propagation [20]. Power loss was also due to the increase in exhaust back-pressure introduced by the turbocharger, adding to pumping losses [10]. The added utilisation of exhaust gases driving the compressor resulted in a net reduction in waste energy, as seen in Figure 15b. Fifty percent mass flow addition improved efficiency by 2.4%. To avoid power loss at low load, the mass flow factor was set as a variable and activated at 5000 RPM. The successful power profile can be seen in Figure 16. As seen, activation occurs at 5000 RPM and power compensation equal to that of constant turbocharging is seen at increasing loads. This application was applied within all combined technologies instead with a mass flow increase of 50%.

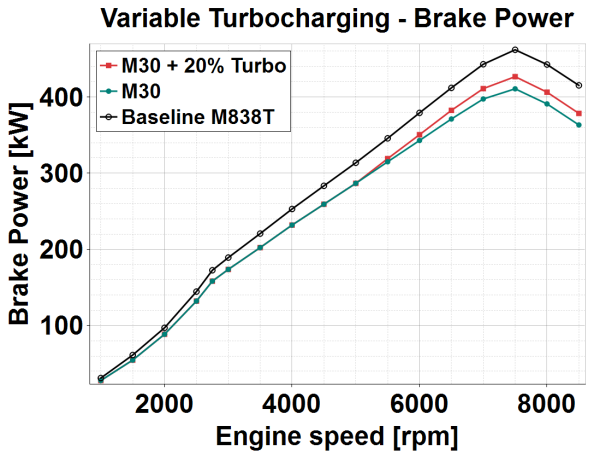


**Figure 16.** Variable turbocharging power output at 5000 RPM.

The emission outputs resulting from the varied turbocharger mass flow and the power output of the final variable turbocharger implementation can be seen Figure 17a,b below:

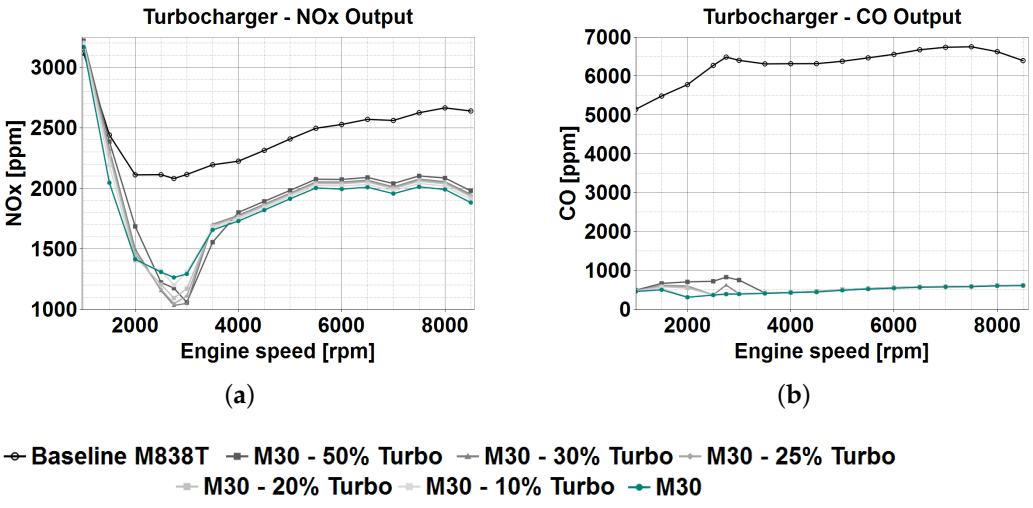


**Figure 17.** Turbocharger impact on emissions. (**a**) NOx; (**b**) CO.

Figure 17 presents the impact of varying magnitudes of turbocharger mass flow increases on both $NO_x$ and CO output. This allows for complete understanding of the combined technologies section. Marginally increased $NO_x$ at higher load was due to the

increased combustion rate, which caused raised cylinder temperature. CO output was increased between 2000 RPM and 3000 RPM due to the excessively lean charge and limited flame propagation. This was caused by the added air massflow, causing added incomplete combustion. CO was unaffected past this point and as such was removed by variable turbocharging.

### *3.7. Miller Cycle Comparison*

Figure 18 illustrates cylinder temperatures and pressures of both Miller cycles at medium load, supporting comparisons made in Sections 3.4 and 3.5.

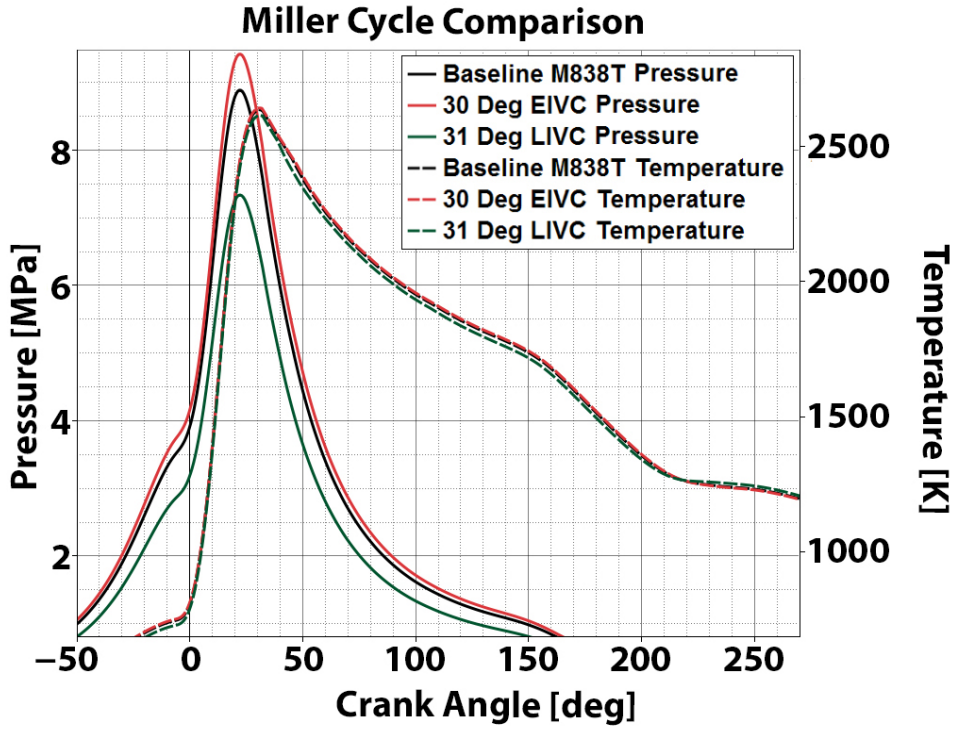


**Figure 18.** Miller cycle pressure and temperature comparison.

As seen from previous discussion, a significant increase to pressure is observed wih the EIVC across all crank angles (8% at peak), due to the reduced combustion duration [10]. The resistive pressure increase, prior to TDC, is illustrated here as the increase just before 0 degrees is apparent. A significant decrease in pressure is observed with the LIVC (17% at peak), due to the loss of charge during blowback. Temperature changes were much more marginal: EIVC saw minor increases across combustion and the LIVC decreases. At 220 degrees, the EIVC appear to match the baseline temperature, whereas the LIVC causes a minor temperature increase. It is unclear why. Despite $NO_x$ and CO improvements achieved with LIVC, the EIVC was best suited to the high performance M838T, and as such became the focus of combined technology investigation.

### *3.8. Combined Technologies*

This section details three combinations of the Miller cycle, biofuels and variable turbocharging, seen in Figure 19. They were selected based upon emission reduction and performance impact potential. Table 2 compares these technologies operating exclusively and co-operatively. These technologies have been investigated both with and without turbocharger application, to understand the impact of applying the Miller cycle and biofuels cooperatively. The overall intention was to utilise the increased Octane number of the renewable biofuels with the added pressure induced by the EIVC. Included below is the investigation of three combinations, with and without turbocharging.

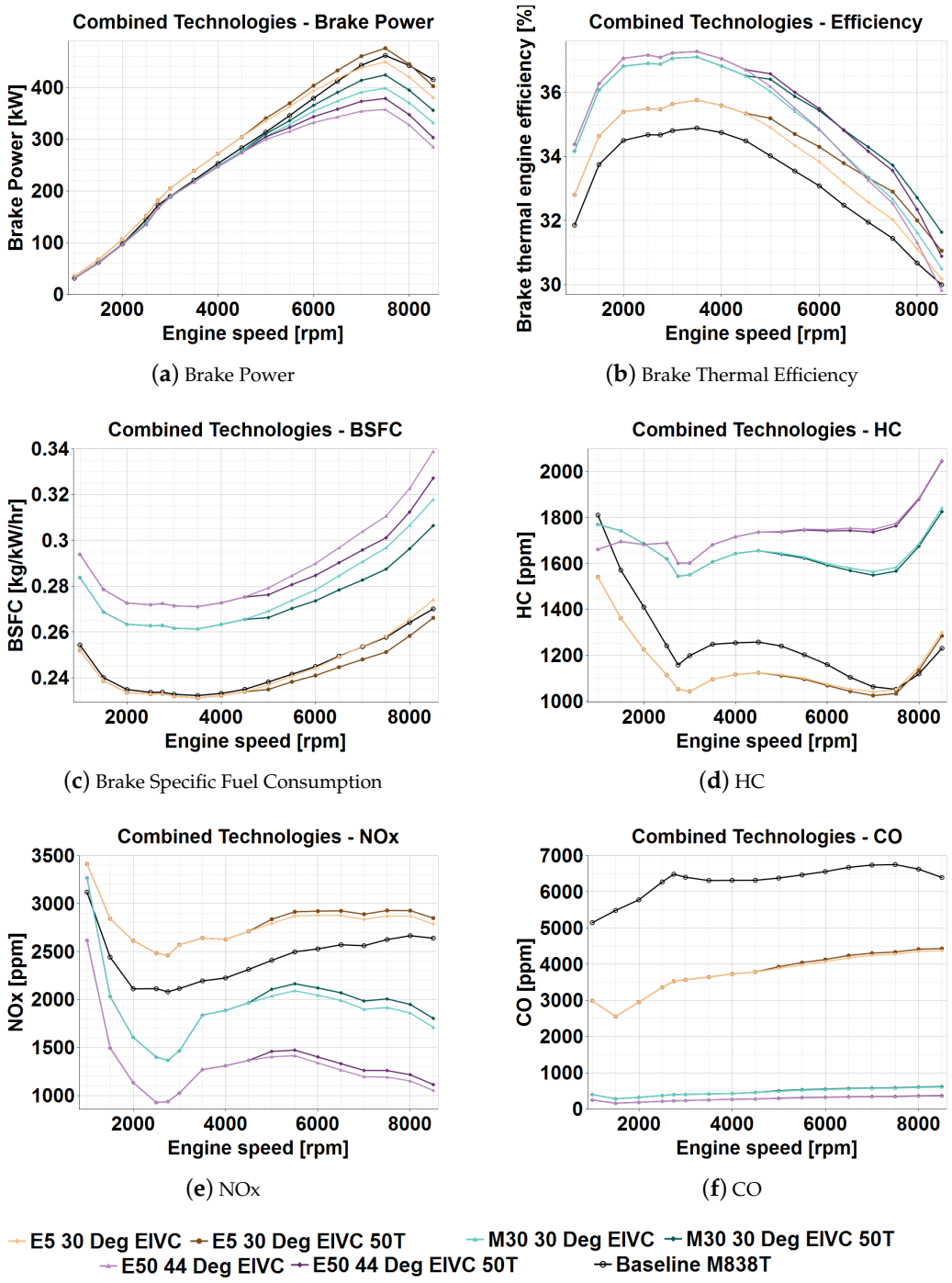


**Figure 19.** Combined technology outputs.

**Table 2.** Summary Results of all Promising Combined and Individual Technologies.

| Technology | Power (kW) | | EFFB (%) | | BSFC (kg/kWh) | | $NO_x$ | CO | HC |
|---|---|---|---|---|---|---|---|---|---|
| | 3500 RPM | 7500 RPM | 3500 RPM | 7500 RPM | 3500 RPM | 7500 RPM | | 7500 RPM | |
| M5 | −0.2 | −2.0 | +0.8 | +0.6 | +0.001 | +0.001 | +15% | -42% | −1% |
| M30 | −18.4 | −51.0 | +2.1 | +1.3 | +0.030 | +0.039 | −23% | −91% | +46% |
| M40 | −27.2 | −75.2 | +2.5 | +1.3 | +0.045 | +0.059 | −60% | −96% | +66% |
| E5 | +0.5 | +0.05 | +0.7 | +0.6 | 0 | 0 | +11% | -36% | −3% |
| E40 | −17.6 | −48.7 | +2.0 | +1.3 | +0.029 | +0.037 | −19.5% | −90% | +42% |
| E50 | −24.6 | −65.2 | +2.2 | +1.3 | +0.040 | +0.051 | −47% | −95% | +56% |
| 30 Deg EIVC | 17.7 | −12.4 | +0.12 | 0 | 0 | −0.001 | −2% | −3% | +3% |
| 44 Deg EIVC | 24.3 | −43.4 | +0.17 | −0.1 | −0.001 | +0.001 | −6% | −6% | +12% |
| 31 Deg LIVC | −42.7 | −38.8 | −0.5 | −0.3 | +0.004 | +0.003 | −3% | −1% | +10% |
| E5 + 30 EIVC | +18.3 | −12.41 | +0.87 | +0.59 | −0.001 | +0.0004 | +9% | −37% | 0% |
| M30 + 30 EIVC | −2.37 | −63.07 | +2.21 | +1.23 | +0.029 | +0.0391 | −27% | −92% | +51% |
| E50 + 44 EIVC | −3.69 | −104.5 | +2.39 | +1.09 | +0.039 | +0.0529 | −55% | −95% | +69% |

#### 3.8.1. Combination 1—E5, 30 Deg EIVC and 50% Turbo

With turbocharging, BSFC, HC and CO output, power and efficiency were all improved across most loads. E5 and 30 degree EIVC without turbocharging affected most factors by the sum of the individual technologies' impact, showing no limitations (Table 2). A compound effect was also observed, such that the combined impact on a factor was greater than the sum of the individual technologies. Efficiency at low load improved by 0.87% compared to the expected 0.82%. This is likely due to the combination of increased pressure provided by the EIVC alongside ethanol's increased octane number. With turbocharging applied this combination provided improvements for all factors excluding $NO_x$, see Figure 19.

#### 3.8.2. Combination 2—M30, 30 Deg EIVC and 50% Turbo

With turbocharging, this combination achieved the highest efficiency at high load (2.3% increase), 50% $NO_x$ reductions and near zero CO output, see Figure 19. The BSFC increase was counteracted by the 30% reduction in gasoline, as such the net gasoline usage and $CO_2$ output was reduced. M30 and 30 degree EIVC without turbocharging caused negative compounding at low load, −2.37 kW power impact compared to the expected −0.7 kW, 92% CO reduction compared to the expected 94% and 51% HC output increase compared to the expected 49% (Table 2). This is likely due to the increased pressure opposing the piston prior to TDC from the EIVC (Figure 18), combined with reduced combustion time of methanol limiting positive pressure post TDC. $NO_x$ has however achieved a positive 2% compounding effect, due to the combined reduced heating value of methanol and charge loss with EIVC.

#### 3.8.3. Combination 3—E50, 44 Deg EIVC and 50% Turbo

With turbocharging, this combination achieved the largest efficiency increase at peak (2.2%) and power loss (17.8%). $NO_x$ and CO saw the largest reductions of 52% and 95%, respectively, thus this combination is ideal for manufacturers to limit environmental impact. Despite the 16.3% BSFC increase, the blend contains 50% less by mass of gasoline and as such the net gasoline consumption and $CO_2$ output was reduced. E50 and 44-degree EIVC without turbocharging showed 4.1 kW higher than expected power at high load, due to increased octane number, with 3.3 kW lower than expected at low load. $NO_x$ again showed a 2% compound improvement (Table 2).

## 4. Conclusions

This report has comprehensively investigated the impact of both EIVC and LIVC Miller cycles, through VVT, on the M838T engine. Incremental investigations were carried out with intake valve profiles of varying early/late closure magnitude. This work targeted application of the Miller cycle on a high performance engine (M838T), with speeds exceeding 7500 RPM. Engines of this power are not widely considered in past research, as such these investigations provide a potential solution for motorsport manufacturers to reduce

environmental impact of their power units. Utilising a 30 degree early closure the EIVC achieved increased cylinder pressure and reduced combustion duration. This resulted in a 17.7 kW power output increase through medium engine loads and loss of 12.4 kW at rated speed. Alongside this, there was an improvement in efficiency of 0.13% and BSFC of 0.4% at low and medium loads. Increases to $NO_x$ and CO output of 5% and 2.5% were observed at low and medium loads, with reductions at rated speed of 2% and 2.2%. The 31-degree LIVC, however, proved less successful, loss of charge resulted in reductions to power (21%) and efficiency (0.5%) across all engine loads. Unburned fuel levels increased and as such HC output and BFSC increased by 300 ppm and 5 g/kWh. $NO_x$ and CO outputs were however reduced across medium loads by 11% and 8.7%, respectively. These findings could be further investigated by iterating in small increments around the promising 30 and 44 degree EIVC, as found within this work these profiles yielded the most progressive results. Alterations could also be carried out to the peak valve opening, this has potential to further increase cylinder pressure with the EIVC and limit the negative blowback effect for the LIVC found in this work.

The biofuels methanol and ethanol were applied, with varying mass fractions, as blends with gasoline to the M838T. High mass fraction blends of these biofuels with gasoline within engines of this power are not widely considered in past research. This work has therefore provided unique information to be utilised by motorsport organisations and manufacturers to reduce environmental impacts of their races and power units. As any number of the investigated blends could be adopted in future motorsport campaigns, 100% fractions proved viable, with power output penalty of 35% for ethanol and 52% methanol. Both CO and $NO_x$ emissions were reduced to near zero. All blends achieved a net reduction in fossil fuel usage and carbon output, despite BSFC increases. The E5 blend achieved improvements to power of 0.5 kW at low and medium loads and efficiency of 0.7%. CO output was also reduced by 36% at the cost of an 11% NOx increase. Increasing biofuel fractions targeted further emission reductions: M30 and E50 achieved $NO_x$ reductions of 23% and 47% alongside CO depletion of 91% and 95%, respectively. At a cost, power was reduced at peak by 51 kW and 65 kW respectively, although both blends improved efficiency by 2.1%. As for the Miller cycle, further investigations may decide to increment more concisely around the more promising M40 and E50 blends. Works may also decide to 100% or near mass fraction blends with lower power engines, in which performance loss is not of concern. This has potential to reduce environmental impact to near zero for average consumer vehicles. Work may also be carried out to investigate multiple fuels within blends, incorporating alternative fuels such as hydrogen with the blends investigated in this report.

The concurrent application of biofuel/gasoline blends with the Miller cycle, has not previously been considered in past literature. This work has therefore proved to be a breakthrough in its understanding. It has potential to provide manufacturers of both high performance and typical consumer power units aiming to meet future environmental legislative targets an unconventional and promising solution. Applied co-operatively the biofuels and Miller cycle EIVC largely improved/limited factors by the sum of the individual technologies. The E5 blend with the EIVC saw efficiency improvements of 0.05% larger than expected. M30 and E50 with EIVC saw compounded improvement of $NO_x$ emissions of 2% and power at rated speed of 0.9% for E50. Compound increases of CO and HC by 2% were however seen. Combined with this was a turbocharger mass flow increase of 50% above 5000 RPM. 7.3% power compensation was achieved at rated speed. This corrected both air intake loss for the EIVC and efficiency loss for the biofuels at high load. As such, the combined technologies achieved a further 1% efficiency and 10 g/kWh BSFC improvement. As the quantity of combinations that could potentially be investigated is limitless, further research can use these base findings to decide which blends and Miller cycles to combine. The most promising results from this finding can be used as a basis. Combination of the EIVC with hydrogen may also be a focus of further work, the

compounded reduction in $NO_x$ output may be particularly beneficial for hydrogen as the high flame propagation speed makes it a primary drawback.

**Author Contributions:** L.O.: Carried out prior research, 'WAVE' modelling of technologies and simulations, analysed and plotted data and wrote final report; Y.W.: Correspondence and supervision throughout, provided instruction and critical feedback of all work also reviewed and edited report. All authors have read and agreed to the published version of the manuscript.

**Funding:** This research received no external funding.

**Conflicts of Interest:** The authors declare no conflicts of interest.

## Abbreviations

The following abbreviations are used in this manuscript:

| | |
|---|---|
| EIVC | Early Intake Valve Close |
| LIVC | Late Intake Valve Close |
| $NO_x$ | Oxides of Nitrogen |
| CO | Carbon Monoxide |
| HC | Hydrocarbons |
| $CO_2$ | Carbon Dioxide |
| GHG | Greenhouse Gas |
| VVT | Variable Valve Timing |
| TDC | Top Dead Centre |
| BDC | Bottom Dead Center |
| Deg | Degrees |
| PMEP | Pump Mean Effective Pressure |
| BSFC | Brake Specific Fuel Consumption |
| EFFB | Brake Thermal Efficiency |
| CFD | Computational Fluid Dynamics |
| SI | Spark Ignition |
| DI | Direct Injection |
| RPM | Rotations per Minute |
| M10 or E10 | Denotes a fuel blend consisting of 10% of methanol/ethanol with 90% gasoline (used to describe all blends) |

## References

1. Kasting, J.F.; Ackerman, T.P. Climatic consequences of very high carbon dioxide levels in the Earth's early atmosphere. *Science* **1986**, *234*, 1383–1385. [CrossRef] [PubMed]
2. United Nations: Conference of the Parties. Paris agreement. In *Report of the Conference of the Parties to the United Nations Framework Convention on Climate Change (21st Session, 2015: Paris)*; Retrived December; United Nations: Le Bourget, France, 2015; Volume 4, p. 2017.
3. Clear Air Technology Center. *Nitrogen Oxides (NOx): Why and How They Are Controlled*; Diane Publishing: Darby, PA, USA, 1999.
4. Solomon, S.; Qin, D.; Manning, M.; Chen, Z.; Marquis, M.; Averyt, K.B.; Tignor, M.; Miller, H.L. Climate Change 2007: Synthesis Report. In *Contribution of Working Group I, II and III to the Fourth Assessment Report of the Intergovernmental Panel on Climate Change*; IPCC: Geneva, Switzerland, 2007.
5. European Comission. *An EU Strategy to Reduce Methane Emissions*; European Comission: Brussels, Belgium, 2020.
6. Rogelj, J.; Den Elzen, M.; Höhne, N.; Fransen, T.; Fekete, H.; Winkler, H.; Schaeffer, R.; Sha, F.; Riahi, K.; Meinshausen, M. Paris Agreement climate proposals need a boost to keep warming well below 2 C. *Nature* **2016**, *534*, 631–639. [CrossRef] [PubMed]
7. DECC. *2013 UK Greenhouse Gas Emissions, Final Figures*; National Statistics Newport: Wales, UK, 2015.
8. Demirci, O.K.; Uyumaz, A.; Sarıdemir, S.; Çınar, C. Performance and Emission Characteristics of a Miller Cycle Engine. *Int. J. Automot. Eng. Technol.* **2018**, *7*, 107–116. [CrossRef]
9. Huang, Z.M.; Shen, K.; Wang, L.; Chen, W.G.; Pan, J.Y. Experimental study on the effects of the Miller cycle on the performance and emissions of a downsized turbocharged gasoline direct injection engine. *Adv. Mech. Eng.* **2020**, *12*. [CrossRef]
10. Pan, X.; Zhao, Y.; Lou, D.; Fang, L. Study of the Miller Cycle on a Turbocharged DI Gasoline Engine Regarding Fuel Economy Improvement at Part Load. *Energies* **2020**, *13*, 1500. [CrossRef]
11. Wang, Y.; Lin, L.; Zeng, S.; Huang, J.; Roskilly, A.P.; He, Y.; Huang, X.; Li, S. Application of the Miller cycle to reduce NOx emissions from petrol engines. *Appl. Energy* **2008**, *85*, 463–474. [CrossRef]
12. Liu, S.; Clemente, E.R.C.; Hu, T.; Wei, Y. Study of spark ignition engine fueled with methanol/gasoline fuel blends. *Appl. Therm. Eng.* **2007**, *27*, 1904–1910. [CrossRef]

13. Wu, T.N.; Chang, C.P.; Wu, T.S.; Shen, Y.H. Emission characteristics of ethanol blending fuels from a laboratory gasoline engine. In *Applied Mechanics and Materials*; Trans Tech Publications Ltd.: Bäch SZ, Switzerland 2013; Volume 253, pp. 2227–2230.
14. Qi, D.; Liu, S.Q.; Zhang, C.H.; Bian, Y.Z. Properties, performance, and emissions of methanol-gasoline blends in a spark ignition engine. *Proc. Inst. Mech. Eng. Part D J. Automob. Eng.* **2005**, *219*, 405–412. [CrossRef]
15. Devi, G.K.; Chozhavendhan, S.; Jayamuthunagai, J.; Bharathiraja, B. Conversion of Biomass to Methanol and Ethanol. In *Horizons in Bioprocess Engineering*; Springer: Cham, Switzerland, 2019; pp. 61–72.
16. Guan, W.; Wang, X.; Zhao, H.; Liu, H. Exploring the high load potential of diesel–methanol dual-fuel operation with Miller cycle, exhaust gas recirculation, and intake air cooling on a heavy-duty diesel engine. *Int. J. Engine Res.* **2021**, *22*, 2318–2336. [CrossRef]
17. Ricardo. Ricardo's WAVE Software, Information and Licensing. Available online: https://software.ricardo.com/products/wave (accessed on 1 August 2020).
18. Wu, C.; Puzinauskas, P.V.; Tsai, J.S. Performance analysis and optimization of a supercharged Miller cycle Otto engine. *Appl. Therm. Eng.* **2003**, *23*, 511–521. [CrossRef]
19. Stephen Bernard, S. *Investigation on Performance, Combustion and Emission Characteristics of a Turbocharged Low Heat Rejection DI Diesel Engine with Extended Expansion Concept*; SAE Technical Paper; SAE International: Warrendale, PA, USA, 2009; p. 28.
20. Efthymiou, P.; Davy, M.; Garner, C.; Hargrave, G.; Rimmer, J.; Richardson, D.; Harris, J. An optical investigation of a cold-start DISI engine startup strategy. In *Internal Combustion Engines: Performance, Fuel Economy and Emissions*; Elsevier: Amsterdam, The Netherlands, 2013; pp. 33–52.
21. Iliev, S. A comparison of ethanol and methanol blending with gasoline using a 1-D engine model. *Procedia Eng.* **2015**, *100*, 1013–1022. [CrossRef]
22. Elfasakhany, A. Investigations on the effects of ethanol–methanol–gasoline blends in a spark-ignition engine: Performance and emissions analysis. *Eng. Sci. Technol. Int. J.* **2015**, *18*, 713–719. [CrossRef]
23. Chehroudi, B. *Hydrocarbon Emission from Spark-Ignited Engines*. Available online: https://www.academia.edu/26659074 (accessed on 1 November 2020).
24. Swithenbank, J. *Combustion Fundamentals*; Technical Report; Department of Fuel Technology and Chemical Engineering, The University of Sheffield: Sheffield, UK, 1970.
25. Wei, H.; Shao, A.; Hua, J.; Zhou, L.; Feng, D. Effects of applying a Miller cycle with split injection on engine performance and knock resistance in a downsized gasoline engine. *Fuel* **2018**, *214*, 98–107. [CrossRef]
26. ProfessCars. *ProfessCars' 2015 McLaren MP4-12C engine Horsepower/Torque Curve*. Automobile-Catalogue. Available online: https://www.automobile-catalog.com/curve/2015/1457915/mclarenmp4-12c.html (accessed on 1 November 2020).
27. Li, Q.; Jin, W.; Huang, Z. Laminar flame characteristics of C1–C5 primary alcohol-isooctane blends at elevated temperature. *Energies* **2016**, *9*, 511. [CrossRef]
28. Larfeldt, J. Technology options and plant design issues for fuel-flexible gas turbines. In *Fuel Flexible Energy Generation*; Elsevier: Amsterdam, The Netherlands, 2016; pp. 271–291.
29. Zhao, H.; Ge, Y.; Tan, J.; Yin, H.; Guo, J.; Zhao, W.; Dai, P. Effects of different mixing ratios on emissions from passenger cars fueled with methanol/gasoline blends. *J. Environ. Sci.* **2011**, *23*, 1831–1838. [CrossRef]
30. Masum, B.; Masjuki, H.; Kalam, M.; Fattah, I.R.; Palash, S.; Abedin, M. Effect of ethanol–gasoline blend on NOx emission in SI engine. *Renew. Sustain. Energy Rev.* **2013**, *24*, 209–222. [CrossRef]
31. Shuai, S.J.; Wang, Y.; Li, X.; Fu, H.; Xiao, J. Impact of octane number on fuel efficiency of modern vehicles. *SAE Int. J. Fuels Lubr.* **2013**, *6*, 702–712. [CrossRef]
32. Mechadyne, R.A.A. Part Load Pumping Losses in an SI Engine. Available online: https://www.mechadyne-int.com/reference/throttle-less-operation/part-load-pumping-losses-in-an-si-engine/ (accessed on 1 January 2021).
33. Akma, T.N. Miller Cycle Combustion Strategy for Downsized Gasoline Engines. Ph.D. Thesis, Loughborough University, Loughborough, UK, 2017.
34. He, X.; Durrett, R.P.; Sun, Z. Late intake valve closing as an emissions control strategy at Tier 2 Bin 5 engine-out NOx level. *SAE Int. J. Engines* **2009**, *1*, 427–443. [CrossRef]